CrystEngComm

Accepted Manuscript

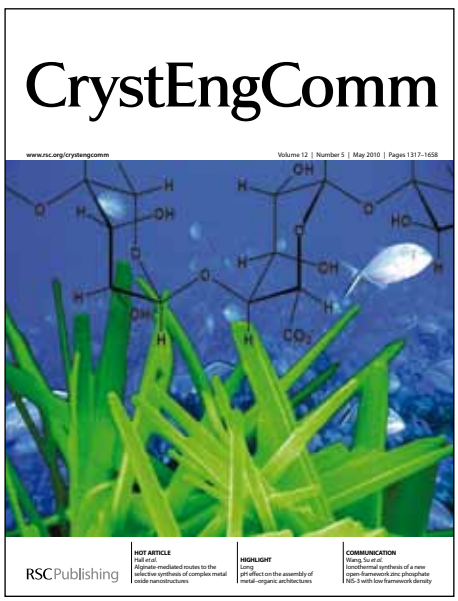

Cite this: DOI: 10.1039/c0xx00000x

www.rsc.org/xxxxxx

PAPER

Facile bubble-assisted evaporation-induced assembly of high-density arrays of Co_3O_4 nano/microlotus leaves: fluorescent properties, drug delivery, and biocompatibility

Guo-Xiu Tong,*[,†] Fang-Ting Liu,[†] Wen-Hua Wu,[†] Chao-Li Tong,[†] Ru Qiao,[†] Hui-Chen Guo*[‡]

Received (in XXX, XXX) Xth XXXXXXXXX 20XX, Accepted Xth XXXXXXXXX 20XX
DOI: 10.1039/b000000x

High-density arrays of Co_3O_4 nano/microlotus leaves with excellent fluorescent properties and biocompatibility were synthesized using a facile bubble-assisted evaporation-induced approach and its potential application in drug delivery was assessed. The morphologically controlled growth of Co_3O_4 nano/microlotus leaf arrays could be realized by evaporating the acetone solution of cobalt nitrate hexahydrate in a tunable kinetic procedure, in which the gas bubbles generated in-situ in the reaction system directed the assembly of the crystal coatings and/or the nuclei. These nano/microlotus leaf arrays were characterized by field-emission scanning electron microscope (FE-SEM), X-ray energy dispersive spectroscopy (EDX), X-ray diffraction (XRD), X-ray photoelectron spectrum (XPS), transmission electron microscopy (TEM), and nitrogen adsorption/desorption and Brunauer-Emmett- Teller (BET). Fluorescein isothiocyanate (FITC) loaded into these nano/microlotus leaf arrays was used as a model platform to assess its efficacy as a drug delivery tool. Its release kinetic study revealed a two-step release pattern of FITC from the nano/microlotus leaf arrays for over 24 h, with a burst release of around 83.4 % dye just within a few hours. We envision that these Co_3O_4 nano/microlotus leaf arrays, with the hierarchically porous structures and high efficacy to adsorb chemicals such as the fluorescent dye FITC, could serve as a delivery vehicle for controlled release of chemicals administered into live cells, opening potential to a diverse range of applications including drug storage and release as well as metabolic manipulation of cells.

Introduction

Recently micro/nanocontainers, with unusual morphologies like bowls, bottles, cups, lotus leaves, have attracted much attention considering their unique applications.[1–3] Such applications include photocatalytic activities, nanosensors, nanoreactors,[4] biomedical and nanofluidic devices,[5] nanosphere selection,[6] controlled releaseas,[7] microelectronics,[8] coercivity enhancement,[9] as well as plasmonic devices for enhancing electromagnetic fields.[10] Various synthesis strategies have been used to construct micro/nanocontainers, including the template method,[2] the milling-etching technique,[8] nanosphere lithography, the sputtering technique,[9] and chemical polymerization.[4] However, some unavoidable disadvantages (i.e., the complicated multi-steps, high-cost, low yields and unfavorable harsh reaction conditions) limit its extensive application. Therefore, a rational, simple, highly efficient, and low-cost method for fabricating complex, oriented micro/nanocontainers like a lotus leaf (preferably via a self-assembly mechanism) is still significantly challenging to develop.

Due to its simplicity, high efficiency, and low cost, the evaporation-induced self-assembly strategy has the potential to construct organic and/or inorganic materials into micro/nanostructures with a range of well-defined morphologies and large-scale.[11] Up to date, successful synthesis of some particular micro/nanostructures have involved polypyrrole nanoparticles,[12] colloidal crystals,[13] thin films,[14] Au nanorods,[15] hierarchically structured porous silica,[16] mesoporous Co_3O_4 nanowire arrays,[17] and CdSe nanorings,[18] However, novel nano/microlotus leaf arrays obtained from this evaporation-induced self-assembly technique have not yet been reported so far.

Cobalt oxide (Co_3O_4), an important P-type semiconductor, has attracted much research interest because of its intriguing properties and potential applications. Numerous efforts have been made and several methods have been attempted to synthesize Co_3O_4 nanostructured materials with different morphologies, such as nano-leaves,[19] hollow spheres,[20] nanorods,[21] nanowires,[22] nanotubes,[23] nanowalls,[24] and nanoflowers.[25] Nevertheless, to the

†College of Chemistry and Life Sciences, Zhejiang Normal University, Jinhua 321004, People's Republic of China
Corresponding authors. Tel.: +86-579-82282269; Fax: +86-579-82282269. E-mail address: tonggx@zjnu.cn (G.X. Tong) ; ghch-2004@hotmail.com(H.C. Guo)
‡State Key Laboratory of Veterinary Etiological Biology and Key Laboratory of Animal Virology of Ministry of Agriculture, Lanzhou Veterinary Research Institute, Chinese Academy of Agricultural Sciences, Xujiaping 11, Lanzhou, Gansu 730046, China
Electronic supplementary information (ESI) available: SEM images of Co_3O_4 microlotus leaf arrays formed for 6h and SEM image and XRD pattern of Co_3O_4 microspheres. See DOI:

best of our knowledge, Co_3O_4 nano/microlotus leaf arrays are so far unavailable.

Herein, a bubble-assisted evaporation-induced self-assembly have been successfully developed to prepare lotus leaf-like Co_3O_4 microcontainer arrays for the first time. Morphological evolution from nano/microlotus leaf arrays, to nanotubes, and eve to nanowalls, can handily be modulated by changing only the reaction temperature and time. In this reaction process, the in-situ generated gas bubbles (H_2O, O_2, NO_2) directed the assembly of the crystal coatings originating from the evaporation of acetone solvent. The fluorescent properties, drug delivery, and biocompatibility of the Co_3O_4 nano/microlotus leaf arrays have been investigated further.

Experimental Section

Reagent and Materials

All reagents obtained from Shanghai Hengxin Chemical Reagent Co. Ltd. China were analytical reagent and used without any further purification.

Synthesis of Co_3O_4 nano/microlotus leaf arrays

In a typical procedure, 0.75 g of cobalt nitrate hexahydrate was dissolved in 7.5 mL of acetone, and then the mixed solution was placed on a culture plate of 9 cm in diameter and allowed to evaporate at room temperature for about 2 h. The final Co_3O_4 products were obtained by further calcining the above intermediates at 180 °C for 5 h and then at 300 °C for 30 min. A series of experiments were carried out at various evaporation time (0.5 h, 1 h, 2 h, 5 h, and 6 h) and evaporating temperatures (room temperature, 50 °C, and 150 °C) in order to modulate the morphology and size of the resulting products.

Characterization of Samples

The morphology and chemical composition of the as-prepared samples were examined by field-emission scanning electron microscope (FE-SEM, Hitachi S-4800, 10 kV) and energy dispersive X-ray spectroscopy (EDX, Horbia EX-250, 20 kV) associated with FE-SEM, respectively. Crystalline phase and structure were identified by X-ray diffraction (XRD) using a D/MAX-IIIA diffractometer with CuKα radiation (λ = 0.15406 nm) and high-resolution transmission electron microscopy (HRTEM, JEM-2100F, 200 kV). The surface elemental compositions were measured by X-ray photoelectron spectroscopy (XPS, XSAM800, Kratos Ltd, UK) with a monochromatic Mg Ka (1253.6 eV) X-ray source and a pressure of 5–7×10^{-9} mbar. The X-ray gun was operated at 180 W (12 kV, 15 mA). All XPS data were corrected with the binding energy of C1s at 285.0 eV. Nitrogen adsorption-desorption isotherms were obtained on a nitrogen adsorption apparatus (ASAP 2020M Micromeritics instruments, USA). The samples are degassed at 150 °C prior to Brunauer-Emmett-Teller (BET) measurements. The BET specific surface area (S_{BET}) is determined by a multipoint BET method by using the adsorption data in the relative pressure P/P_0 range of 0.05–0.25. The pore size distribution was derived from the desorption isotherm using the Barret-Joyner-Halender method.

Photoluminescence test

The photoluminescence spectrum was measured by a RF-5301PC spectrofluorophoto meter (ShiMADZU) by using a Xe arc lamp as the excitation source at room temperature. The excitation wavelength for the PL measurement was 325 nm.

Loading of FITC into Co_3O_4 nanoparticles

FITC (Fluorescein isothiocyanate) was used as a model drug and the effect of particle morphology on drug loading was studied. 10 mg/mL of Co_3O_4 nanoparticles was mixed with 1 mL of 1 mg/mL FITC in acetone solution. The mixture was then incubated for different time duration at ambient temperature, followed by centrifugation at 5000 rpm for 5 min. FITC was quantified, using a UV-vis spectrophotometer, according to its absorbance peak at 488 nm. Raw data were converted to concentration (μg/mg) of FITC using the standard curves obtained at different time point.

Release profiles of FITC from Co_3O_4 nanoparticles

The FITC-loaded Co_3O_4 nanoparticles were mixed with 1 mL of PBS (pH 5.2) and then incubated at ambient temperature under gentle shaking. A 100-μL aliquot of supernatant was removed at a given time after centrifugation at 5000 rpm for 5 min and this was supplemented with 100 μL of fresh PBS. The absorbance of FITC at 488 nm was recorded, and the cumulative release of FITC was calculated. One-way ANOVA and Duncan's multiple-range test for post hoc comparisons were carried out, and α = 0.05 significant level was used.

In vitro cytotoxicity tests

Hela cells were collected and diluted to a cell density of 1×10^5/mL in complete medium, and then seeded into 96-well plates (100 μL/well). After cultured for 24 hours, the nanoparticles with different concentrations (25, 50, 100, 200, 500, 1000 μg/mL) were added to the cells and the cells were incubated

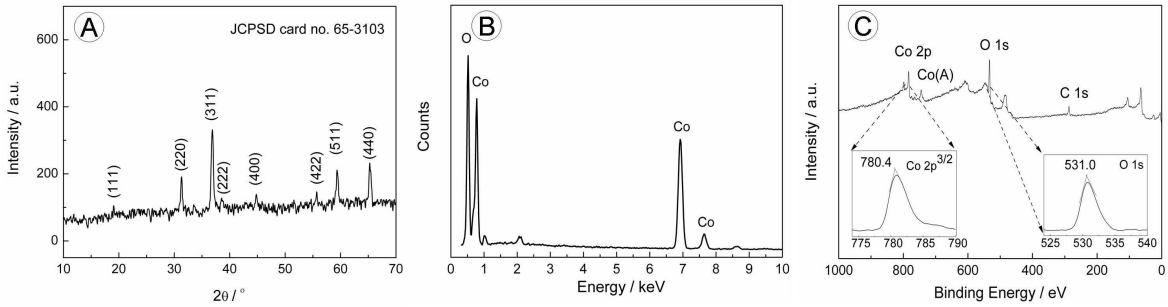

Figure 1. (A) XRD pattern, (B) EDX spectrum, and (C) XPS spectrum of the typical products.

at 37 °C for 48 h. The cells were washed to remove the unbound nanoparticles. The cell viability was measured by using the Cell Titer 96 aqueous one solution assay (Promega, Madison, WI) and was expressed as a percentage of the control.

Results and discussion

The phase structures and compositions of the typical products were characterized by X-ray diffraction (XRD), energy dispersive spectroscopy (EDX), and X-ray photoelectron spectroscopy (XPS), respectively. All the XRD peaks (Figure A) in the range of 10 °<2θ<70 ° can accurately be indexed as (111), (220), (311), (222), (400), (422), (511), (440), and (533) directions of face-centered cubic Co_3O_4 spinel structure (a =0.8056 nm, Fd3m, JCPSD card no. 65-3103). No characteristic peaks of impurities, such as CoO, Co_2O_3 or Co, are detected, suggesting single-phase Co_3O_4. The EDX spectrum confirmed the presence of Co and O with an atomic Co to O ratio of about 0.75 (Figure 1B). The wide survey XPS spectrum (Figure 1C) showed that the O1s binding energy in the bottom right inset was 531.1 eV, consistent with a previous report[26]. In contrast, the photoelectron line located at 780.3 eV in the bottom left inset was apropos to the Co3/2p of Co_3O_4 (CAS Registry No. 1308061). These results revealed that high purity Co_3O_4 was easily grown using the present method.

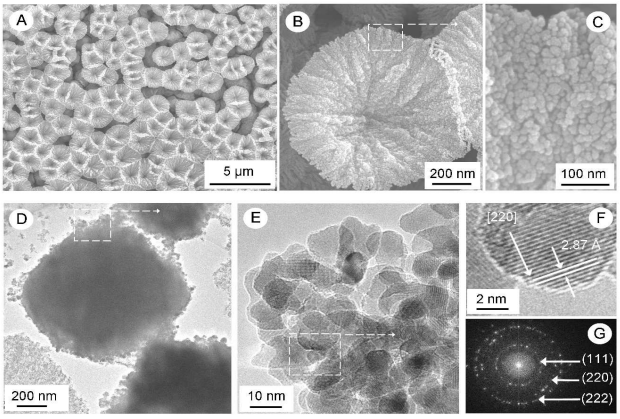

Figure 2. Lotus leaf-like Co_3O_4 arrays. (A) low- and (B−C) high-magnification SEM images, (D) typical TEM image, (E) enlarged TEM image highlighted by the square in (D), (F) HRTEM image highlighted by the square in (E), and (G) fast Fourier translation (FFT) pattern in (E).

The SEM image (Figures 2A and 2B) showed that the products were lotus leaf-like Co_3O_4 microcontainers 1.5−2.0 μm in size, were uniformly arranged, and had high densities of 5−6 × 10^5 units·mm^{-2}. The enlarged SEM image (Figure 2C) showed that these microlotus leaves consisted of numerous nanoparticles with diameters of 5−15 nm, which was further confirmed by the TEM images (Figures 2D and 2E). The HRTEM image of a nanoparticle (Figure 2F) depicted a fringe spacing of 0.287 nm that corresponded to the (220) plane. The fast Fourier translation (FFT) of the entire highlighted region in Figure 2E was shown in Figure 2G. As indexed, all face-intervals calculated from the diffraction rings exactly corresponded to the dependent crystal faces of Co_3O_4. The clear diffraction rings suggested that the Co_3O_4 microlotus leaves were polycrystalline.

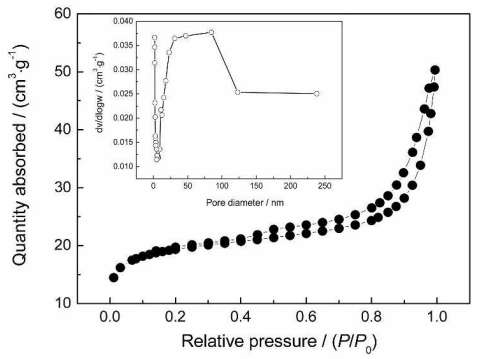

Figure 3. Nitrogen adsorption/desorption isotherms and the corresponding pore size distribution curves (in the inset) of the lotus leaf-like Co_3O_4 microcontainer arrays.

Nitrogen isotherms of physical adsorption/desorption (Figure 3) show that the Co_3O_4 microlotus leaf arrays had type IV isotherms with H3 hysteresis loops according to the Brunauer–Deming–Deming–Teller classification[27]. The S_{BET} was 66.31 $m^2 \cdot g^{-1}$. The pore size distribution as depicted in the inset of Figure 3 was wide because of the peculiar nanostructure. The micropores and small mesopores were related to the primary aggregation of the nanoparticles, whereas the larger mesopores and macropores were associated with the secondary organization of the nanoparticles as well as to the hollow structures inside the microlotus leaves. Indeed, the formation of hierarchical nanopore structures on a multilength scale was highly conducive to the adsorption and transportation of a chemical reagent.

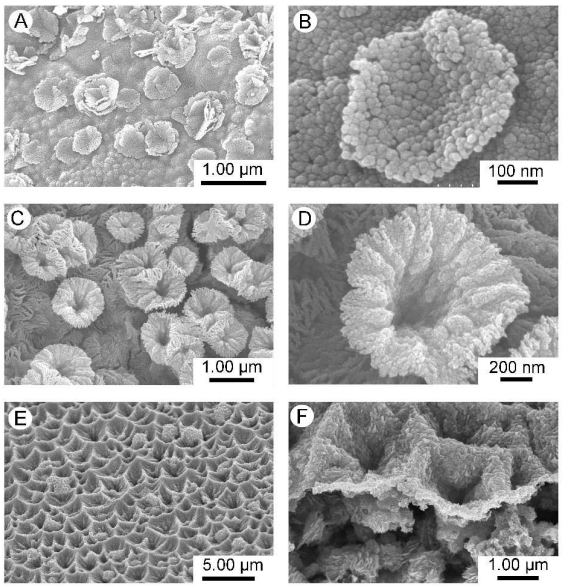

Figure 4. FESEM images of the samples obtained via evaporating acetone on a culture plate at room temperature. The evaporation times were 0.5 h (A) and (B), 1 h (C) and (D), and 5 h (E) and (F). The next step involved calcination at 180 °C for 5 h, and then at 300 °C for 30 min.

To determine the formation mechanism, the effects of various factors (evaporation time, evaporating temperature, and solvent) on the dimension and morphology of the resulting products were investigated. The results showed that within a short evaporation

time (ca. 0.5 h), massive nanolotus leaves 300−600 nm in size and composed of ca. 10 nm nanoparticles were sparsely distributed on the surface at a density of 6−7 × 10^5 units·mm^{-2} (Figures 4A and 4B). Interestingly, Co_3O_4 arrays of thinly scattered microlotus leaves with diameters of ca. 1.0 μm and density of 2−3 × 10^6 units·mm^{-2} were produced with increased evaporation time to about 1 h (Figures 4C and 4D). The size and distribution density of the Co_3O_4 microlotus leaves in the arrays significantly increased to 1.5−2.0 μm and decreased to 5−6 × 10^5 units·mm^{-2}, respectively, when the evaporation time lengthened to 2 h (Figure 2A). Interestingly, compact Co_3O_4 microlotus leaves 2–3 μm in diameter formed at a density of 2−3 × 10^5 units·mm^{-2} when evaporation time increased to 5 h (Figures 4E and 4F) or more (See Figure S1 in Supporting Information). This finding demonstrated that the size and density of the microlotus leaves can be easily modulated by altering the evaporation time. Lengthening evaporation time help the increased diameter and distribution density of lotus leaves took on an inverted U-shaped change trend.

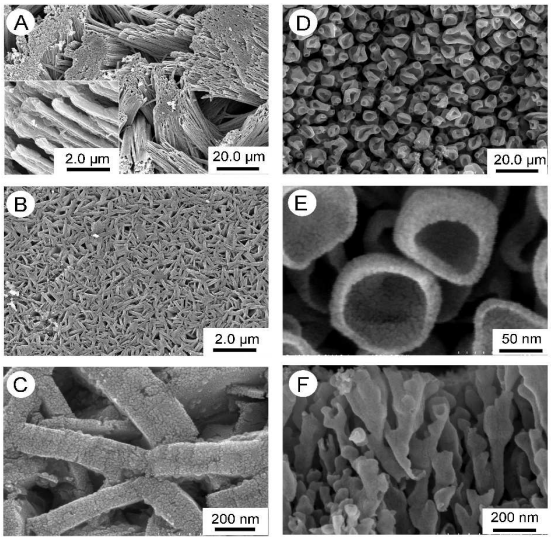

Figure 5. FESEM images of the samples obtained via evaporating the acetone solution placed on a culture plate at the relatively high temperature of: (A) at 50 °C for 5 h, and (B, C) at 150 °C for 5 h, respectively. The next step involved calcination at 180 °C for 5 h and then at 300 °C for 0.5 h. Top view with (D) the low- and (E) high-magnifications and (F) tilted side view of the Co_3O_4 nanomaterials obtained via directly decomposing $Co(NO_3)_2.6H_2O$ at 180 °C for 5 h, followed calcination at 300 °C for 0.5 h.

Besides, with increased evaporation temperature to 50 °C and even to 150 °C, arrays of nanorods and nanowalls were produced instead of lotus leaf-like products (Figure 5A–C). Regarding the solvent effect, only arrays of some distorted or deformed tube-shaped nanostructures were produced in the absence of acetone. These nanostructures were orderly arranged perpendicularly to the substrate (Figure 5D–F). Overall, the above morphological evolution results accurately validated our proposed mechanism of a bubble-assisted, evaporation-induced self-assembly process (Scheme 1).

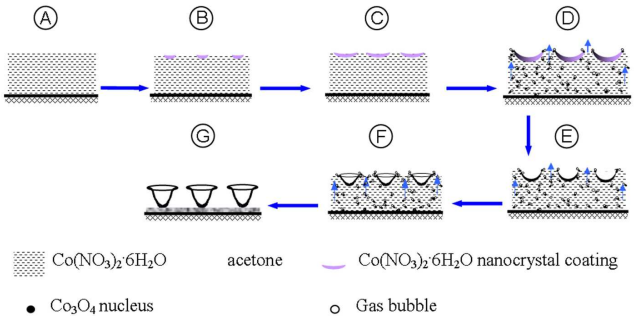

Scheme 1 Generation of high-density lotus leaf-like Co_3O_4 arrays.

Generally, the formation of micro/nanostructure arrays is ascribed to the template method,[2] the milling-etching technique,[8] nanosphere lithography, the sputtering technique,[9] and chemical polymerization.[4] In our experiments, no shape-directing agent or template was introduced into the reaction system. Only solvent evaporation was involved in the reaction, and large amounts of gas (including O_2, H_2O, and NO_2) were released, as shown in Reaction (1). Therefore, the formation of arrays of high-density Co_3O_4 microlotus leaves is possibly correlated with solvent evaporation and gas release. Scheme 1 illustrates the growth procedure for arrays of high-density Co_3O_4 microlotus leaves, which involves three major steps. First, $Co(NO_3)_2·6H_2O$ grains dissolved in acetone cover a culture plate (Scheme 1A). Second, after the acetone on the solution surface evaporated, $Co(NO_3)_2·6H_2O$ concentration on the surface gradually increases until local supersaturation is reached. $Co(NO_3)_2·6H_2O$ then nucleates and grows, and causes the appearance of a considerable stack of lotus leaf-like nanocrystal coatings on the surface (Scheme 1B). These lotus leaf-like nanocrystal coatings progressively develop with prolonged evaporation time, causing an increase in the size and distribution density of the nanolotus leaves. When evaporation time rose to a certain value (i.e., 2 h), the decreased density was because some nanolotus leaves grew up via swallowing up neighboring ones. A longer evaporation time corresponds to larger and denser lotus leaf-like nanocrystal coatings, which may even combine with one another. Subsequently, bigger and denser microlotus leaf arrays are formed after calcinations. Third and last, the intermediate products are further calcined at a relatively high temperature to obtain the Co_3O_4 samples. The high temperature allows for the thermal decomposition of $Co(NO_3)_2·6H_2O$ and the evaporation of residual acetone, as illustrated by the following complex chemical reaction:

$$3Co(NO_3)_2 \cdot 6H_2O \xrightarrow{\Delta} Co_3O_4 + O_2\uparrow + 6NO_2\uparrow + 18H_2O\uparrow \quad (1)$$

The calcination process obviously caused the Co_3O_4 nuclei to combine with a large amount of gas bubbles including O_2, NO_2, and H_2O. These gas bubbles take the Co_3O_4 nuclei to the solution surface to form the Co_3O_4 microlotus leaves (Scheme 1 D–F). This phenomenon is explained on one hand by the gas bubble upward driving force perpendicular to the base, which makes the lotus leaf-like nanocrystal coatings turn upward. On the other hand, these coatings grow at the edges via the mass transportation of continually generated Co_3O_4 nuclei induced by the in-situ-generated gas bubbles. As a result, vertically aligned arrays of Co_3O_4 microlotus leaves are formed. In our previous work, the

bubble-engaged assembly strategy has been developed for the preparation of Fe nanostructure (nanotubes, hollow spheres, nanofibers),[28,29] complex ferric oxide nanostructures,[30] and arrays of Co_3O_4 nanotubes.[31] Our group is currently in the process of similarly applying this bubble-engaged assembly method for synthesizing arrays of nanorods, nanowalls, nanotubes, and nanobowls.

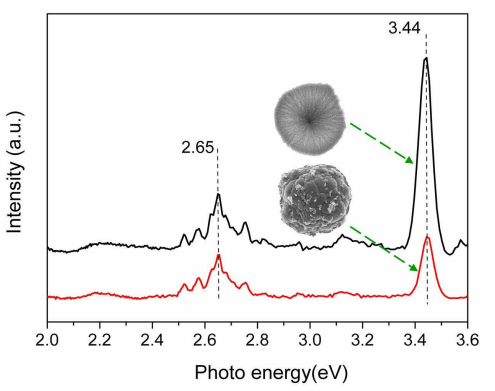

Figure 6. Photoluminescence emission spectrum of the lotus leaf-like Co_3O_4 microcontainers arrays and Co_3O_4 microspheres.

The optical property of the Co_3O_4 microlotus leaf arrays was characterized by a fluorescence spectrometer with an excitation wavelength of 325 nm. From Figure 6, we can clearly observe that there are two luminous zones, located in 360 nm (3.44 eV) and 450–500 nm (2.51–2.76 eV), respectively, which apparently differ from the single luminous band in the reported literatures, and are obviously higher than those of the bulk Co_3O_4 (about 1.6 eV),[26] Co_3O_4 thin films (about 1.65–2.2 eV),[32] and Co_3O_4 nanowires (ca. 2.07 eV).[23,24] The blue-shift of the energy band gap in our case is ascribed to the size quantization effects,[33] as well as the special morphology and microstructure of the Co_3O_4 microlotus leaf arrays with polycrystalline structure.[34] A contrast test reveals that the Co_3O_4 microlotus leaf arrays exhibits higher fluorescence intensity than Co_3O_4 microspheres in the same measure condition. Co_3O_4 microspheres were obtained via the thermal decomposition of cobalt nitrate hexahydrate at 700 °C for 1 h (See Figure S2 and S3 in Supporting Information). This interesting phenomenon may be related to the gain effect of the lotus leaf-like morphology on the fluorescence. The aforesaid gain effect exhibits not only the highly effective collection to the incident ray but also enhanced radiation to the excited ray.

The nanomedicine is recognised as an emerging field with enormous potential for developing new therapeutic concepts. A range of nanoscale materials have been explored in the last few years for drug delivery to address the problems associated with conventional drug therapies such as limited drug solubility, poor biodistribution, lack of selectivity and unfavourable pharmacokinetics. Among them, nanoporous materials (i.e., nanoporous alumina, titania nanotubes, porous silicon, hydroxyapatite etc.) with ordered and controlled pore structures, high specific surface area and pore volume have attracted great attention, particularly for implantable drug delivery systems.[35,36] Here we used fluorescein isothiocyanate (FITC) as a model drug to study the controlled drug delivery done by Co_3O_4 microlotus leaf arrays.

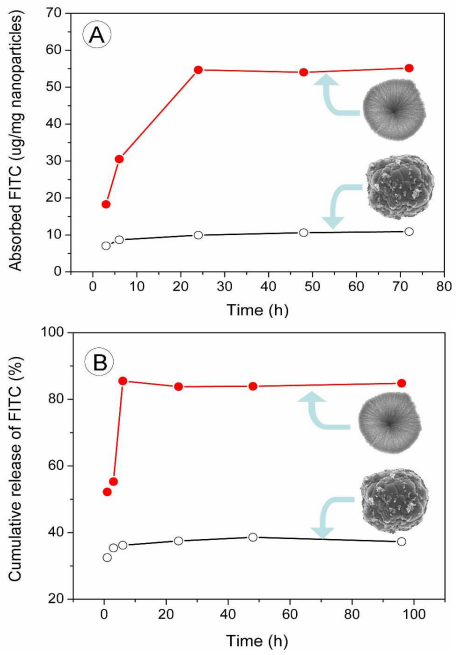

Figure 7. Kinetics of FITC (A) adsorption on and (B) cumulative release from the lotus leaf-like Co_3O_4 microcontainers arrays and Co_3O_4 microspheres.

Figure 7A show the kinetics of FITC adsorption on the Co_3O_4 microlotus leaf arrays. FITC dye dissolved in acetone at a concentration of 10 mg/mL was mixed with Co_3O_4 samples for several days in order to observe the relationship between time and the absorbance of FITC. The data seem to suggest that there is a two-step loading pattern, with a rapid absorbance of the dye attained in the first 6 h and a second relatively slow loading phase occurring in the subsequent 18 h. It demonstrates the absorbance of FITC to the Co_3O_4 microlotus leaf arrays is correlative to time point in 24 h. The equilibrium capacity at 24 h is 54.68 and 9.95 μg of FITC per mg of the Co_3O_4 microlotus leaf arrays and Co_3O_4 microspheres, respectively. This indicates that the binding of FITC is dependent on the morphology of Co_3O_4 nanoparticles, as seen by the higher adsorption amount of FITC onto Co_3O_4 microlotus leaf arrays than Co_3O_4 microspheres. The high absorbance amount is associated with the as-made microlotus leaf arrays with hierarchical nanopores and high specific surface area, which favor the adsorption and transportation of the chemical reagent. In addition, the above result also suggests that the encapsulation of FITC is a diffusion-driven process.

The release studies of FITC from the Co_3O_4 microlotus leaf arrays (10 mg/mL) at room temperature were conducted in inorganic solution of PBS (pH 5.2). PBS (pH 5.2) was used to assess whether fluorescent dye could be released from Co_3O_4 nanoparticles before their entry into cell. A pH value of 5.2 was chosen to mimic the physiological pH values inside endosomes. Figure 7B shows the cumulative release kinetics of FITC from the Co_3O_4 microlotus leaf arrays and microspheres. Obviously, the release rate of FITC from the Co_3O_4 microlotus leaf arrays is very rapid, showing a two-step release pattern with a rapid initial burst release and a subsequent relatively slow sustained release over 24 h. The initial burst release observed in the first 6 h is around 83.4 % of the dye, which is significantly higher than

40.2 % from the Co_3O_4 microspheres. The aforesaid two-step release pattern and high cumulative amount are related to the hierarchically porous structures. Indeed, this could be incorporated in our future work for controlled release by changing the morphology of the nanoparticles.

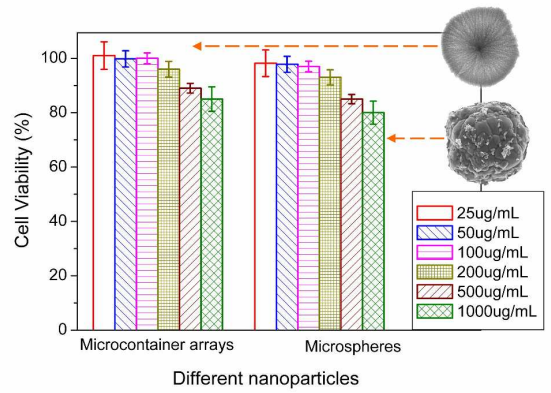

Figure 8. Influences of different concentrations of the lotus leaf-like Co_3O_4 microcontainers arrays and Co_3O_4 microspheres on the cell viability, respectively.

MTS assay is used to determine the proliferation and viability of cells that has been treated with different concentrations of the Co_3O_4 nanoparticles. Figure 8 shows the densities of cells cultured with different concentrations of Co_3O_4 microlotus leaf arrays and Co_3O_4 microspheres for 48 h, respectively. Even though cell viability was observed to decrease as a function of concentration, it was noted that none of the cell samples reached below 80 % of viability. As such, this indicates that even at a high concentration of 1000 μg/mL, the Co_3O_4 microlotus leaf arrays exert no significant cytotoxic effect on the cells and thus presents as a safe and ideal delivery vehicle or chemical/drugs into cells.

Conclusions

In summary, a facile bubble-assisted evaporation-induced process has been developed to synthesize high-density arrays of uniform Co_3O_4 microlotus leaves. The results disclose that Co_3O_4 arrays consist of microlotus leaves with diameter of 1.5–2.0 μm in a high density of 5–6×10^5 units·mm^{-2}. Furthermore, the Co_3O_4 microlotus leaf arrays present enhanced fluorescent properties, which are of great importance to apply in recording material, an infrared photoconductive detector, and for nonlinear infrared optics, optoelectronic applications, etc. Additionally, FITC adsorption studies reveal that the arrays of Co_3O_4 microlotus leaves have a high adsorption capacity for FITC at high concentration of the nanoparticles. Their release kinetics show that FITC adsorbed onto these Co_3O_4 microlotus leaf arrays could be released continually over 24 h in organic solution, whereas burst release kinetics of the fluorescent dye was observed just within a few hours. Also, the synthesized Co_3O_4 microlotus leaves exhibit good biocompatibility with Hela cells. Thus, this work demonstrated the potential of producing the microlotus leaf arrays as a carrier for protein/drug delivery for imaging and other biomedical applications.

ASSOCIATED CONTENT

Supporting Information

AUTHOR INFORMATION

Corresponding Authors

*E-mail: tonggx@zjnu.cn (G. X. TONG); ghch-2004@hotmail.com (H.C. Guo)

Notes

The authors declare no competing financial interest.

Acknowledgements

This work is financially supported by the National Natural Scientific Foundation of China (51102215 and 31100688), Chinese Scholarship Council (201208330114), Natural Scientific Foundation of Zhejiang Province (Y4100022), Teacher Training Project of Zhejiang Normal University (KYJ06Y12134), and National Innovation and Entrepreneurship Training Program of Undergraduates (201310345016).

References

(1) U. K. Gautam, Y. Bando, J. H. Zhan, P. M. F. J. Costa, X. S. Fang and D. Golbergy, *Adv. Mater.*, 2008, **20**, 810.
(2) J. Peng, X. Li, D. H. Kim and W. Knoll, *Macromol. Raipd Commun.*, 2007, **28**, 2055.
(3) Y. F. Wang, J. H. Zhang, X. L. Chen, X. Li, Z. Q. Sun, K. Zhang, D. Y. Wang and B. Yang, *J. Colloid Interface Sci.*, 2008, **322**, 327.
(4) L. T. Qu, G. Q. Shi, F. E. Chen and J. X. Zhang, *Macromolecules* ,2003, **36**, 1063.
(5) A. K. Srivastava, S. Madhavi, T. J. White and R. V. Ramanujan, *J. Mater. Chem.*, 2005, **15**, 4424.
(6) X. Wang, E. Graugnard, J. S. King, Z. Wang and C. J. Summers, *Nano Lett.*, 2004, **4**, 2223.
(7) V. Bajpai, P. G. He and L. Dai, *Adv. Funct. Mater.*, 2004, **14**, 145.
(8) J. Y. Yuan, L. T. Qu, D. Q. Zhang and G. Q. Shi, *Chem. Commun.*, 2004, **8**, 994.
(9) T. Ito and S. Okazaki, *Nature*, 2000, **406**, 1027.
(10) J. Ye, P. V. Dorpe, W. V. Roy, G. Borghs and G. Maes, *Langmuir*, 2009, **25**, 1822.
(11) C. J. Brinker, Y. F. Lu, A. Sellinger and H. Y. Fan, *Adv. Mater.*, 1999, **11**, 579.
(12) J. Jang and J. H. Oh, *Langmuir*, 2004, **20**, 8419.
(13) D. D. Brewer, J. Allen, M. R. Miller, J. M. De Santos, S. Kumar, D. J. Norris, M. Tsapatsis and L. E. Scriven, *Langmuir*, 2008, **24**, 13683.
(14) M. A. Wahab, S. Sudhakar, E. Yeo and A. Sellinger, *Chem. Mater.*, 2008, **20**, 1855.
(15) X. M. Zhang and T. Imae, *J. Phys. Chem. C*, 2009, **113**, 5947.
(16) H. Y. Fan, S. Reed, T. Baer, R. Schunk, G. P. López and C. J. Brinker, *Micropor. Mesopor. Mat.*, 2001, **44**, 625.
(17) Y. G. Li, B. Tan and Y. Y. Wu, *J. Am. Chem. Soc.*, 2006, **128**, 14258.
(18) J. X. Chen, W. S. Liao, X. Chen, T. L. Yang, S. E. Wark, D. H. Son, J. D. Batteas and P. S. Cremer, *ACS Nano*, 2009, **3**, 173.
(19) L. R. Meng, W. M. Chen, C. P. Chen, H. P. Zhou and Q. Peng, *Chin. Phys. Lett., 2010,* **27**, 128101.
(20) C. H. Chen, S. F. Abbas, A. Morey, S. Sithambaram, L. P. Xu, H. F. Garces, W. A. Hines and S. L. Suib, *Adv. Mater.*, 2008, **20**, 1205.
(21) L. Li, Y. Li, S. Y. Gao and N. Koshizaki, *J. Mater. Chem.*, 2009, **19**, 8366.
(22) K. T. Nam, D. W. Kim, P. J. Yoo, C. Y. Chiang, N. Meethong, P. T. Hammond, Y. M. Chiang and A. M. Belcher, *Science*, 2006, **312**, 885.
(23) X. W. Lou, D. Deng, J. Y. Lee, J. Feng and L. A. Archer, *Adv. Mater.*, 2008, **20**, 258.
(24) T. Yu, Y. W. Zhu, X. J. Xu, Z. X. Shen, P. Chen, C. T. Lim, J. T. L. Thong and C. H. Sow, *Adv. Mater.*, 2005, **17**, 1595.

(25) Y. G. Zhang, Y. C. Chen, T. Wang, J. H. Zhou and Y. G. Zhao, *Micropor. Mesopor. Mat.*, 2008, **114**, 257.
(26) J. Van Elp, J. L. Wieland, H. Eskes, P. Kuiper, G. A. Sawatzky, F. M. F. de Groot and T. S. Turner, *Phys. Rev. B*, 1991, **44**, 6090.
(27) K. S. W. Sing, D. H. Everett, R. A. W. Haul, L. Moscou, R. A. Pierotti, J. Rouquérol and T. Siemieniewska, *Pure & Appl. Chem.*, 1985, **57**, 603.
(28) G. X. Tong, J. G. Guan, Z. D. Xiao, F. Z. Mou, W. Wang and G. H. Yan, *Chem. Mater.*, 2008, **20**, 3535.
(29) G. X. Tong, M. Hong, J. G. Guan, J. H. Yuan, W. H. Wu and H. S. Qian, *Micro & Nano Lett.*, 2011, **6**, 722.
(30) G. X. Tong, J. G. Guan, Z. D. Xiao, X. Huang and Y. Guan, *J. Nanopart. Res*., 2010, **12**, 3025.
(31) G. X. Tong, J. G. Guan and Q. J. Zhang, *Adv. Funct. Mater.*, 2013, **23**, 2405.
(32) H. Yamamoto, S. Tanaka, T. Naito and K. Hirao, *Appl. Phys. Lett.*, 2002, **81**, 999.
(33) L. E. Brus, *J. Chem. Phys.*, 1984, **80**, 4403.
(34) A. A. Patel, F. X. Wu, J. Z. Zhang, C. L. Torres-Martinez, R. K. Mehra, Y. Yang and S. H. Risbud, *J. Phys. Chem. B*, 2000, **104**, 11598.
(35) D. Losic and S. Simovic, *Expert. Opin. Drug Del*, 2009, **6**, 1363.
(36) E. Gultepe, D. Nagesha, S. Sridhar and M. Amiji, *Adv. Drug Deliver. Rev.*, 2010, **62**, 305.

BRIEFS

High-density arrays of biocompatible Co_3O_4 microcontainers with unique fluorescent properties have been successfully prepared via a facile bubble-assisted evaporation-induced assembly.

TOC Graphic